Ge-Sb-Te based phase-change nanoparticles

Chen, Bin

Chapter 3

Crystallization kinetics of Ge-Sb films

Abstract

The crystallization kinetics of phase-change materials (PCMs) entail a crucial aspect of phase-change memory technology and their study is also of interest to advance the understanding of crystallization in general. Research on crystallization of PCMs remains challenging because of the short (nanosecond) time and small (nanometer) length scales involved. Ultrafast differential scanning calorimetry (DSC) offers a powerful tool to study crystallization via ultrahigh heating rates. Here, we used this tool to study the crystallization kinetics of growth-dominant Ge_7Sb_{93}. Two models describing the viscosity of the undercooled liquid were used to interpret the data and were subsequently crosschecked by independent growth-rate data. With both models the data in Kissinger plots could be fitted well, but one of the models resulted in large discrepancy with the independent data. These results demonstrate that great care is needed when deriving crystal-growth rates from ultrafast DSC measurements because orders of magnitude errors can be made. The present analysis showed a slightly non-Arrhenius crystallization behaviour for the Ge_7Sb_{93} alloy, corresponding to a fragility of 65 and a glass transition temperature of 379 K. The overall viscosity and growth rate of this alloy between the glass and melting temperatures have been revealed, as well as a maximum growth rate of 21 m s^{-1} at ~800 K. Models based on ultrafast DSC data offer interpretation of crystallization kinetics of PCMs and thereby strongly support the design of PCMs for memory applications.

Based on *Crystallization Kinetics of Supercooled Liquid Ge–Sb Based on Ultrafast Calorimetry,*
B. Chen, J. Momand, P.A. Vermeulen, B. J. Kooi, *Crystal Growth & Design* 16.1, (2015),242.

3.1 Introduction

Memories based on phase-change materials (PCMs) demonstrate promising performances for a next generation memory technology.[1,2] PCMs can be switched rapidly and reversibly between amorphous and crystalline phases, offering large optical and electrical contrast. Lying at the heart of PCMs memory technologies, crystallization has aroused for many years a large number of investigations, e.g. though both experiments[3–10] and molecular dynamics simulations[11–14]. Most of the conventional experimental studies on crystallization of PCMs focused on the relatively low temperature region mainly because of limitations in instrumentation.[3,7–10] For instance, *Friedrich et al.*[10] studied the crystallization temperatures of $Ge_2Sb_2Te_5$ alloy via electrical resistance measurement by employing heating rates (Φ) from 0.53 to 5.3 K min^{-1} and strict Arrhenius behavior of crystal growth was found. Similar results were reported by *Park et al* [3] via differential scanning calorimetry (DSC) with Φ ranging from 5 to 20 K min^{-1}. The crystallization temperatures in these two cases are around 420 K. Crystallization kinetics at higher temperatures is not only of interest for theoretical studies but also remarkably important for the real application of PCMs because, due to the high switching speeds that have to be achieved in the applications, crystallization usually happens at the higher temperatures. However, research providing a comprehensive picture of crystallization kinetics involving these higher temperatures still remains a challenge due to the short time and small length scales involved.

Eising et al.[15] reported a direct method to measure the crystal growth rate at higher temperature for Ge_xSb_{1-x} alloys by employing a high speed optical camera and a laser to accelerate crystallization. The growth rate was measured over 5 orders of magnitude. However, the shortcoming of this method, as generally holds for laser-induced crystallization methods, is that the temperature of the sample cannot be directly measured, making it harder to arrive at a comprehensive picture of crystallization kinetics as a function of temperature. In another work, *Salinga et al.*[16] solved this problem by using a laser to only induce an amorphous mark in a thin film on a heater and then use laser-based time-resolved reflectivity measurements to determine the rate by which the mark recrystallizes from its rim at the known temperature set by the heater. A strict Arrhenius behavior in growth velocity from ~10 nm s^{-1} to ~1 m s^{-1} was observed for melt-quenched AgInSbTe (AIST).

Orava et al.[17] achieved important progress regarding the crystallization kinetics of PCMs at higher temperatures by employing ultrafast differential scanning calorimetry (DSC). In this way a large range of heating rates (from 50 to 40 000 K s^{-1}) can be applied, whereby crystallization in a relatively wide temperature range becomes available. Employing a model for viscosity by *Cohen*

and *Grest* (the CG model),[18] the growth rate for a wide temperature range between glass and melting temperatures was derived. Strong non-Arrhenius behavior in crystallization kinetics of $Ge_2Sb_2Te_5$ (GST) films was discovered, due to fragile liquid behaviour of the (supercooled) liquid phase subjected to crystallization. This indicated a novel and promising approach to study the crystallization kinetics of PCMs at relatively high temperatures. However, the interpretation of the data obtained from ultrafast DSC is rather indirect and not straightforward. For instance, a very simplified description of nucleation and subsequently Johnson-Mehl-Avrami-Kolmogorov (JMAK) theory[19–23] was used to derive the growth rate of GST from the glass transition temperature (T_g) to the melting temperature (T_m). Moreover, directly measured crystal growth rate data were not used to verify the accuracy of their interpretation of the ultrafast DSC data. Meanwhile, the activation energy for growth provided by this model is clearly higher than that from the conventional measurements; see Figure 1 in (News & Views) perspective by *Wuttig et al.*.[24] Also it is readily observable in this figure that the absolute values obtained by this model are at least three orders of magnitude larger than the ones obtained from conventional measurements for the corresponding temperatures. Moreover, in a recent paper, *Orava et al.*[25] adopted the same method to study the crystallization of AgInSbTe, and a mismatch between the modeled Kissinger plot and the experimental data occurred for Φ above 200 K s^{-1}. These results therefore demonstrate that the derivation of the growth rate data from ultrafast DSC measurements has to be tested (more) carefully.

Here we present such an extensive analysis of ultrafast DSC data to comprehend the crystallization kinetics of Ge_7Sb_{93}. Two models (which we designated the MYEGA and CG models; see 3.3.2 for the details) describing the viscosity and growth rate have been adopted to understand the data. Independent growth rate data for the same alloy, obtained by an optical high speed camera where growth was accelerated by a laser, is used to crosscheck the accuracy of our analysis and the validity of the two models. It turns out that the growth rate obtained by the MYEGA model we adopted here leads to a much better match to the data, while that from the CG model shows 2-3 orders of magnitude overestimation of the growth rate at the measurable temperature region by ultrafast DSC. Results show that the MYEGA model for viscosity and growth rate appears appropriate for PCMs. With this model, ultrafast DSC provides us a novel and powerful method to understand the crystallization behavior of PCMs at a higher temperature which is inaccessible by conventional measurements.

3.2 Experimental and analysis methods

Amorphous Ge_7Sb_{93} films with thickness of 200 nm were deposited on glass substrates using co-sputtering with a Unaxis Sputter coater. The deposition rate was 2.5 nm s^{-1}. The films were, without breaking the vacuum, directly capped with a (5 nm) layer of ZnS-SiO_2. More details can be found in our previous work.[26]

Ultrafast heating was then conducted by differential scanning calorimetry for the flakes of the films. They were scraped off from the glass substrate, and then deposited on the active area of a chip sensor (keeping the reference area clean). Heating rates (Φ) in the measurements spanned about three orders of magnitude, i.e. ranged from 50 to 40000 K s^{-1}. The thermal lag between the chip sensor and the phase-change flake is shown in Appendix and it can be seen that the thermal lag dose not influence the shift of the crystallization peak temperature obtained by increasing the Φ.

In this paper, two crystal growth-rate models were adopted to determine the growth rate for the present Ge_7Sb_{93} alloy. These models will be called CG and MYEGA in this article, respectively. Using these models we thus explicitly assume that crystallization occurs in a supercooled liquid. This is expected, but *Salinga et al.*[16] indicated that amorphous PCMs are actually in a glass state and that for crystallization events at relatively low temperatures the phase transition instead might be directly from amorphous to crystalline (without entering the supercooled liquid) phase.

From our previous work we established that the nucleation of Ge_xSb_{1-x} occurs after a certain incubation time and after that only growth of crystal is significant, i.e. we have pre-existing nuclei (site saturation); see Figure 3.7 of the Appendix. Therefore, the main process we are looking at here is the growth of crystals. The number of nuclei per unit (untransformed) volume was therefore assumed to be a constant (N), neither time nor temperature dependent. The same assumption was made in the work of *Orava et al.*.[17,25] However, in their analysis for $Ge_2Sb_2Te_5$ it was not independently checked whether this assumption is justified. Here, we clearly have this justification; see Appendix.

3.3 Results and discussion

3.3.1 DSC traces obtained from experiments and numerical simulations

Figure 3.1a displays direct traces of ultrafast DSC measurements performed on Ge_7Sb_{93} powdered films for heating rates ranging from 50 to 40 000 K s^{-1}. It shows that the crystallization peak temperature (T_p) shifts to higher temperatures for higher Φ, i.e. from 450 K at 50 K s^{-1} to 504 K at 40 000 K s^{-1}. Figure 3.1b shows the numerically simulated DSC traces for the corresponding Φ after

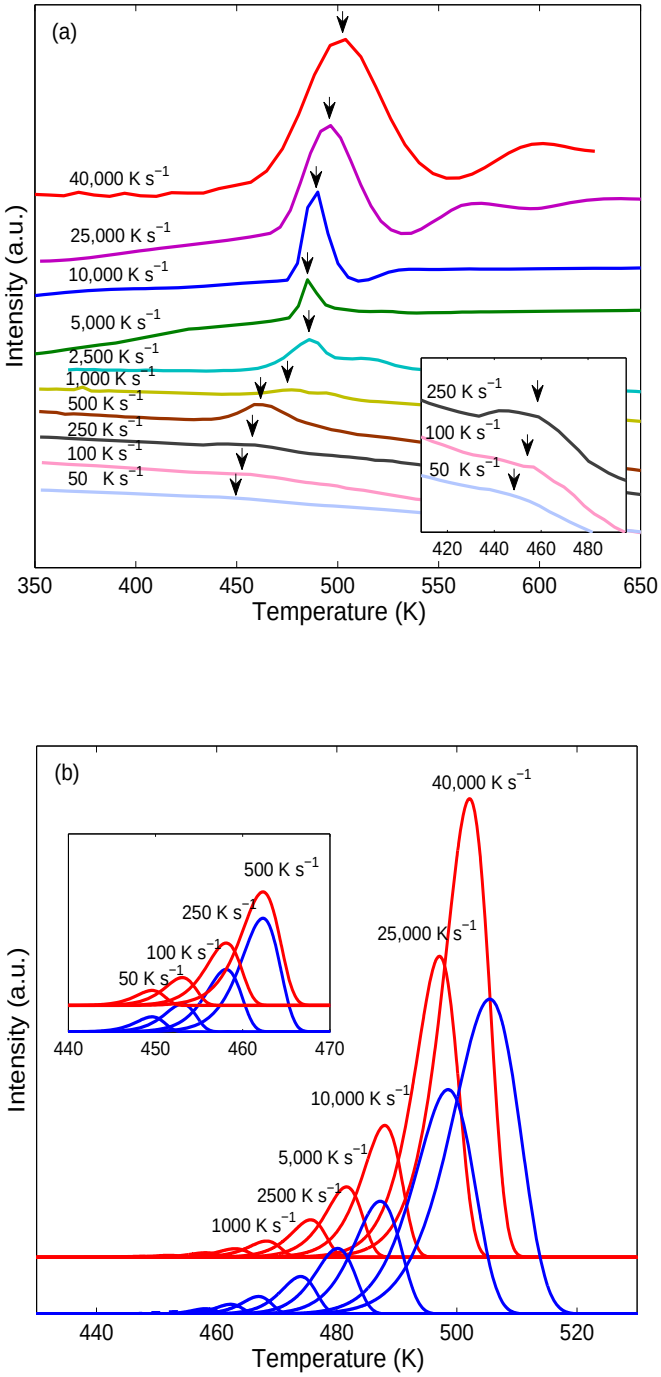

Figure 3.1 Ultrafast DSC traces obtained experimentally and by numerical simulation. The crystallization peak temperatures shift to higher temperature when the heating rate Φ is increased. (a) experimental DSC traces at different Φ, ranging from 50 K s^{-1} to 40 000 K s^{-1}. The T_p are indicated by black arrows. (The magnitude of the exothermic peaks increase with increasing Φ.) (b) Numerically calculated DSC traces by MYEGA (red lines) and CG (blue lines) models for all the Φ used experimentally. Inset shows the zoomed in exothermic peak of the lower Φ. Good match of T_p between the measured data and the calculated data can be observed for both models. Insets show the close-up of the DSC peaks for lower Φ.

fitting data in the Kissinger plot with the MYEGA and CG models. More details about this fitting are provided in the next section. The red curves in Figure 3.1(b) are calculated using the MYEGA model, while the blue curves are from the CG model. In both models T_p shows good agreement with the measured data in Figure 3.1a, with a negligible difference in T_p at higher Φ. For instance, the T_p at 40 000 K s^{-1} is 502.2 K for the MYEGA model and 504.4 K for the CG model. It is worth noting that the (areas under the) exothermic peaks increase significantly with increasing Φ, because the DSC signal is proportional to the Φ.[27] Similar as in the ultrafast DSC traces described in the work of *Orava et al.*,[17] also here the traces do not show any signature of a glass transition (separated from the crystallization peak). This is not generally the case, because in our earlier work on SeTe alloys the glass transition and crystallization were separated well in the ultrafast DSC traces.[28] However, this work also showed that the difference between T_g and T_p decreases and vanishes when the glass forming ability of the alloy becomes poorer and disappears. PCMs of interest for high switching speed applications, like $Ge_2Sb_2Te_5$ and Ge_7Sb_{93}, have to be poor glass formers and therefore in general will not have clearly separated T_g and T_p.

3.3.2 Kissinger plot and fitting of data

According to theory from Kissinger,[29] the activation energy for crystallization (Q) is proportional to the gradient of $\ln(\Phi/T_p^2)$ versus $1/T_p$, as described by Equation 3.1:

$$\frac{Q}{R} = -\frac{d(\ln(\Phi/T_p^2))}{d(1/T_p)} \tag{3.1}$$

with Q the activation energy for crystallization, Φ heating rate, R the gas constant and T_p the peak temperature in the DSC trace. It is straightforward to derive the activation energy for crystallization if we plot $\ln(\Phi/T_p^2)$ versus $1/T_p$ according to Equation 3.1. In traditional DSC measurements, due to the relatively low and narrowly confined Φ, typically a constant activation energy Q is found. As a result, strict Arrhenius behavior with a linear Kissinger plot in crystallization is generally observed.[3,10] In contrast, the Kissinger plot as based on the ultrafast DSC measurements performed here is slightly curved, as shown in Figure 3.2. Note that the data in Figure 3.2 is weighted to be the most representative data in our measurements. As described in the methods section, the T_p remarkably vary in the ultrafast DSC measurements, especially at high Φ. Therefore, the 2-3 data points with lowest T_p values for a certain Φ were given to the most weight to be presented in Figure 3.2, since they correspond to the best thermal contact between the chip sensor and the

Ge_7Sb_{93} flakes. The red solid circles in Figure 3.2 are the experimental data for Φ from 50 K s^{-1} to 40 000 K s^{-1}. Numerical simulations were performed to analyze this curved behavior of the data in the Kissinger plot and subsequently understand the crystallization kinetics of the Ge_7Sb_{93} alloy.

JMAK theory is used to perform numerical simulations to obtain DSC traces along with modeled Kissinger plots. To perform these simulations, the temperature dependence of the crystal growth rate *U(T)* is essential. In this paper, two different models for *U(T)* have been used.

The first one is based on work of *Salinga et al*. (and *Mauro et al*.), in which the growth rate can be written as:[16]

$$U(T) = \frac{4 r_{atom} k_B T}{3\pi\lambda^2 R_{hyd} \eta(T)} [1 - \exp(-\frac{\Delta G(T)}{k_B T})] \tag{3.2}$$

with r_{atom} the atomic radius(~1.5 Å), λ the diffusional jump distance (~1 Å), R_{hyd} the hydrodynamic radius (~0.5 Å), k_B the Boltzmann constant and $\Delta G(T)$ the change of Gibbs free energy. All these above values are the same as were taken for AgInSbTe.[16] According to *Thomson* and *Spaepen*,[30] $\Delta G(T)$ in Equation 3.2 can be estimated from the latent heat of melting (ΔH_m), approximately 0.22 eV at^{-1},[31] and the melting temperature T_m:

$$\Delta G(T) = \frac{\Delta H_m (T_m - T)}{T_m} (\frac{2T}{T_m + T}) \tag{3.3}$$

Where T_m is taken from Ge-Sb phase diagram as 887 K.[32]

Finally, an accurate description of the viscosity $\eta(T)$ is required in Equation 3.2. According to *Mauro et al.*[33] $\eta(T)$ can be modeled for glass-forming liquids as follows:

$$\log_{10}\eta(T) = \log_{10}\eta_\infty + (12 - \log_{10}\eta_\infty)\frac{T_g}{T}\exp[(\frac{m}{12 - \log_{10}\eta_\infty} - 1)(\frac{T_g}{T} - 1)] \tag{3.4}$$

with η_∞ the viscosity at infinite temperature, which is estimated here as: $\log_{10}\eta_\infty = -3$ and m the fragility. The main idea of fitting the experimental data in the Kissinger plot (Figure 3.2) is to adjust the parameters, i.e., T_g , m , and the number density of nuclei *N* (per unit of untransformed space). The best fit (smallest χ^2 value leading to R^2 of 0.924) is shown as the red curve in Figure 3.2, with T_g =379 K, m =65, with a proper value of *N* (for more details, see Appendix). These values are

plausible and consistent, because in a previous study the T_g of Ge_9Sb_{91} and Ge_8Sb_{92} were obtained by an independent method as 395 K and 382 K, respectively.[15] According to *Kalb et al.*[34] T_g is found to be related to the crystallization (peak) temperature T_p in PCMs, ~10 K below T_p when a constant Φ of 40 K min^{-1} was applied to GST and AIST. Therefore, consistent with our finding it is expected that the T_g of Ge_7Sb_{93} is slightly lower than the ones of Ge_9Sb_{91} and Ge_8Sb_{92}, since the T_p of Ge_xSb_{1-x} alloys decreases with the decrement of x.[9] The m of this alloy is 65, which is also close to the ones of Ge_9Sb_{91} and Ge_8Sb_{92} (59 and 61, respectively) as found by an independent method and indicates a trend of slightly increasing m with decreasing Ge concentration.

The other model we used for the growth rate is the same as adopted by *Orava et al.* and it is based on the expression by *Cohen* and *Grest* for the viscosity of glass-forming liquids. *Orava et al.* used this model also for fitting data of $Ge_2Sb_2Te_5$ powdered films in a Kissinger plot and thereby describing the viscosity and growth rate.[17] According to the CG model the kinetic coefficient for crystal growth U_{kin} can be written as:[17]

$$\log_{10} U_{kin} = A - \frac{2B}{T - T_0 + [(T - T_0)^2 + 4CT]^{1/2}} \tag{3.5}$$

with *A, B, C,* T_0 input parameters. Then the real growth rate $U(T)$ as a function of temperature is:[17]

$$U(T) = U_{kin}[1 - \exp(-\frac{\Delta G(T)}{RT})] \tag{3.6}$$

with *R* the gas constant and $\Delta G(T)$ the driving force for crystallization, which in this case is also described by Equation 3.3.

Using the same fitting procedure as for the MYEGA model, the modeled Kissinger plot (the blue curve in Figure 3.2) for the CG model matches well with the experimental data. The best fit we can obtain here offers B =119.2，C =1.5, T_0 =443 K, with R^2 of 0.937. T_0 is supposed to be 10% to 17% higher than the measured T_g,[18] which is 379 K from fitting by the MYEGA model and indeed T_0 is 17% higher than that in this fitting. The parameter *A* in this model (see Equation 3.5) is not relevant for fitting the data in the Kissinger plot, but it is crucial to determine the absolute values of the viscosity and growth rate as function of temperature as will be discussed in the next two sections of this chapter.

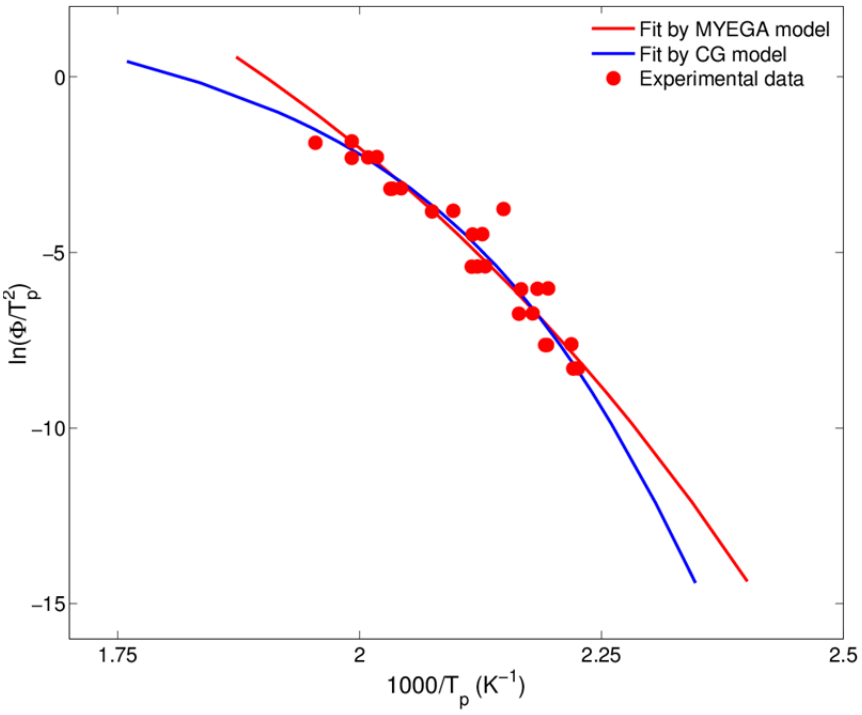

Figure 3.2 Kissinger plot with fittings for the MYEGA and the CG models. The red circles are the most weighted experimental data obtained by ultrafast DSC at Φ from 50 to 40 000 K s^{-1}. The red curve is the modeled Kissinger plot using the MYEGA model for growth rate. The fit quality can be valued by adjusted R^2, 0.924 here. The blue curve is the modeled Kissinger plot using the CG model, with R^2 of 0.937. Taking the scatter in the data into account, these 2 fittings can be considered as good fits. Slight curvature can be seen in Kissinger plot of experimental data as well as the ones of these 2 models. However, the difference in curvature between these 2 models is obvious, as the CG model gives much stronger curvature than the MYEGA model.

3.3.3 Viscosity and fragility

Figure 3.3 shows the viscosity of the Ge_7Sb_{93} flaked films as based on fitting the two models to the data in the Kissinger plot (shown in Figure 3.2). As described by Equation 3.4, the viscosity can be easily obtained once the T_g and m values have been derived from fitting the MYEGA model. Employing these two values obtained in the previous section, the temperature dependence of viscosity is shown as the red line in Figure 3.3, with a m of 65. The region marked in thick red (0.75~0.85 T_g/T) in these lines represents the temperature region that was analyzed using ultrafast DSC measurements of this alloy.

To obtain η and m in the CG model, the kinetic coefficient U_{kin} (Equation 3.5) has to be transposed. By assuming $\eta \propto U_{kin}^{-1}$ and setting $\eta(T_m)$ to 1.2×10^{-3} Pa s with T_m the melting

temperature, the viscosity is obtained shown as the blue, dashed curve. The latter requirement is actually used to determine the (still unknown) value of *A* in Equation 3.5. Note that this model does not provide a value for T_g, so, it is assumed to be 379 K here, as we obtained from the MYEGA model. As can be seen in Figure 3.3, the viscosity at T_g slightly deviates from 10^{12} Pa s, which is a widely accepted value directly associated with T_g for glass forming liquids. This can be a result of the decoupling of $\eta \propto U_{kin}^{-1}$. So we take the decoupled equation $U_{kin} \propto \eta^{-\zeta}$ to derive the viscosity, combined with setting $\eta(T_g)$ to 10^{12} Pa s. The fitted ζ here is 0.97. The blue solid line is the η

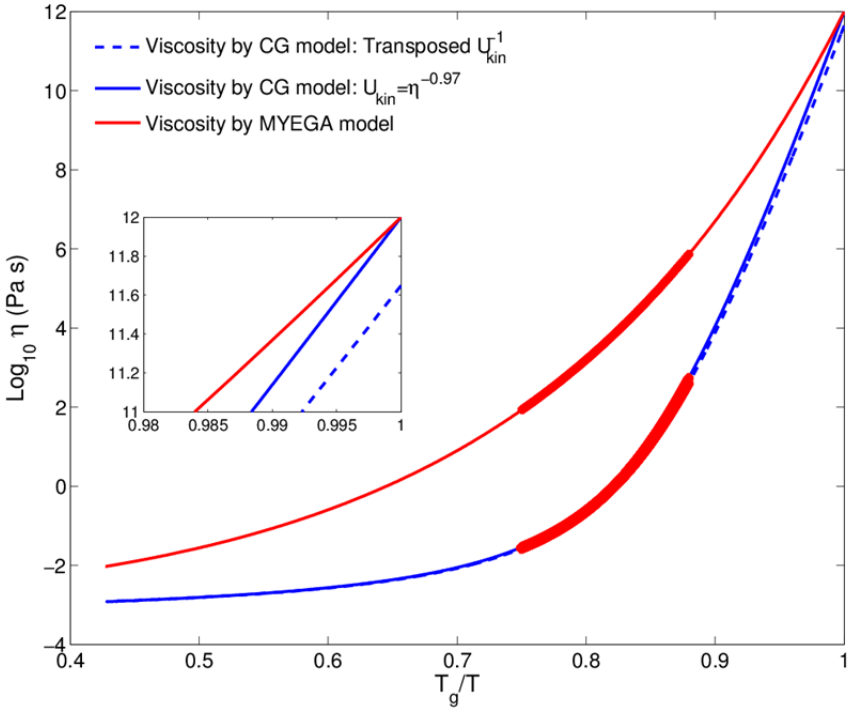

Figure 3.3 Angell plots for temperature dependence of viscosity from MYEGA and CG models. The red line is derived from the MYEGA model, in which the viscosities at T_g and T_∞ are fixed to 10^{12} and 10^{-3} Pa s, respectively. The fragility m is fitted to be 65 for this model, close to the values obtained for Ge_8Sb_{92} and Ge_9Sb_{91} alloys in reference.[15] The blue dashed lines are the viscosity obtained for the CG model by transposing $U_{kin}(\eta \propto U_{kin}^{-1})$ and by using the additional boundary condition $\eta(T_m)=1.2\times10^{-3}$ Pa. Note that in this way the viscosity at T_g is slightly different from 10^{12} Pa s. Then, the $\eta(T_g)$ is set to 10^{12} Pa s by using $U_{kin} = \eta^{-\zeta}$, with ζ=0.97 here, as shown as the blue, solid line. The m is derived to be 86 for this CG model. As can be nicely seen in this figure, the CG model gives steeper curve at T_g, leading to higher m. The thicker red regions on both curves indicate the temperature region in which the peaks temperatures in the ultrafast DSC have been obtained. Inset is the close-up of the area close to T_g.

after the decoupling is taken into account. The *m*, defined as $m = \left.\frac{d(\log_{10}\eta(T))}{d(T_g/T)}\right|_{T=T_g}$, in this case of the CG model applied to this alloy leads to a value of 86 which is thus substantially larger than the *m* obtained by the MYEGA model.

3.3.4. Growth rate

The main purpose of performing ultrafast DSC here is to obtain the overall temperature dependence of growth rate and by doing so also the maximum growth rate of the alloy can be extrapolated. The red curve in Figure 3.4 shows for the MYEGA model the growth rate as function of temperature transposed from the viscosity using Equation 3.2. The non-Arrhenius temperature dependence of the growth rate can be readily observed. In the measured temperature region from ultrafast DSC, i.e. from ~0.5 to ~0.57 T_m (450 K to 505 K, marked in red in Figure 3.4), the derived growth rate matches well with independent data of Ge_7Sb_{93} (the blue squares in Figure 3.4), where crystal growth was measured directly by employing a high-speed optical camera and by accelerating the growth using a laser.[15] The maximum growth rate is readily extrapolated as 21 m s^{-1} at 800 K (~0.90 T_m) from this plot, which is slightly higher than that of Ge_8Sb_{92}, ~15 m s^{-1} previously reported in Ref. 15. *Adelerhof* [35] reported experimental data for the maximum growth rate of $Ge_{10}Sb_{90}$ as 50 m s^{-1} and that for Ge_7Sb_{93} should be higher than 60 m s^{-1} by extrapolating the trend in this paper showing that the growth rate increases with decreasing Ge concentration. However, the materials they studied were melt-quenched alloys, which usually exhibit a higher growth rate than the as-deposited materials we study here. For example, the growth rates of melt-quenched AgInSbTe PCMs are measured 2-3 orders of magnitude higher than the ones of as-deposited AgInSbTe.[16] The maximum growth rate obtained here can therefore readily shift to a value higher than 50 m s^{-1} once the materials become melt-quenched.

It is worth noting that the Stokes-Einstein relation is intrinsically included in Equation 3.2 in the MYEGA model. The growth rate *U* directly relates to the diffusivity *D*, while in Stokes-Einstein equation *D* couples to viscosity η by $D(T) \propto k_B T/\eta(T)$. However, it is well accepted that the Stokes-Einstein equation decouples below ~1.2 T_g,[14,36] i.e. 454 K for this alloy. In Figure 3.4, the modeled growth rate from the MYEGA model matches excellently with the independent data beyond 450 K, while below that some discrepancy arises. This discrepancy can therefore probably stem from the decoupling. With the decoupling considered, we take $U \propto \eta^{-\zeta}$ with ζ =0.9 to calculate the growth rate from 379 K (T_g) to 450 K (~1.2 T_g). The green line in Figure 3.4 shows

the decoupled, modeled growth rate, with a clearly better match to the independent data. The excellent match between our fitting data and the independent data from Ref. 15 demonstrates that the method (with MYEGA model) adopted here to analyze the ultrafast DSC data appears reliable. This suggests a proper method to study the ultrafast DSC measurements and an appropriate model to study the crystallization kinetics of this alloy at relatively high temperatures not reachable with conventional measurement techniques.

Meanwhile, the CG model is also used to evaluate the temperature dependence of growth rate for this alloy. Again, consistently with the previous section, an extra relation is required to determine the value of the parameter *A* in Equation 3.5 in order to obtain the absolute value of the growth rate. Similar to Ref. 17, the effective diffusion coefficient *D* can be derived by Stokes-Einstein equation from viscosity η:

$$D = \frac{k_B T}{3\pi a \eta} \tag{3.7}$$

with a the effective jump distance. Instead of 0.3 nm as in Ref. 17, here we take a = 0.15 nm. For growth dominated by diffusion, the U_{kin} at T_m is given by $U_{kin}(T_m) = D(T_m)/a$. So $U_{kin}(T_m)$ is 54 m s^{-1}, close to the maximum crystallization velocity measured by *Adelerhof* [35] and four times the one of GST (13.5 m s^{-1}).[17] An important factor is that the GeSb alloy is a growth-dominated PCM, whereas GST (such as $Ge_2Sb_2Te_5$) is a nucleation-dominant PCM. Moreover, it is known that the highest crystal growth rates in PCMs have been observed for Sb-rich alloys. Therefore the substantial higher $U_{kin}(T_m)$ derived for the current Ge_7Sb_{93} than for GST is according to expectations. The blue curve in Figure 3.4 is the obtained growth rate via the CG model. The maximum growth rate *U* through extrapolation here is 17 m s^{-1} at 695 K (~0.78 T_m). The values of maximum growth rate obtained from both the MYEGA and CG models are very close, which can also shows the rationality of setting the $U_{kin}(T_m)$ value in the CG model to 54 m s^{-1}.

Nevertheless, as can be clearly observed in Figure 3.4, the growth rate at the measuring temperature range derived from the CG model is unexpectedly 2-3 orders of magnitude higher than the independent data, implying a strong overestimation of the growth rate in this CG model to describe the growth rate under ultrafast DSC in Ge_7Sb_{93} alloy. A possible reason for this large discrepancy could be the parameter *A* in Equation 3.5, which directly affects the real growth rate (and viscosity) of this alloy. So we tried instead to vary the *A* value to obtain a better match to the independent growth rate data. A better match can be found, still not as good as the MYEGA model, however an

unacceptable low maximum growth rate of 0.17 m s^{-1} is then obtained (see Appendix). These present findings thus seriously question the validity of the CG model, at least for the present alloy. Moreover the CG model already requires, even excluding the parameter *A*, three fitting parameters to describe the viscosity, whereas the *Mauro* description only requires two fitting parameters (T_g and m). A final disadvantage of the CG model is that it offers no direct information about the T_g of the alloy. One has to assume a value of T_g when calculating viscosity because T_g is not observed in the ultrafast DSC traces.

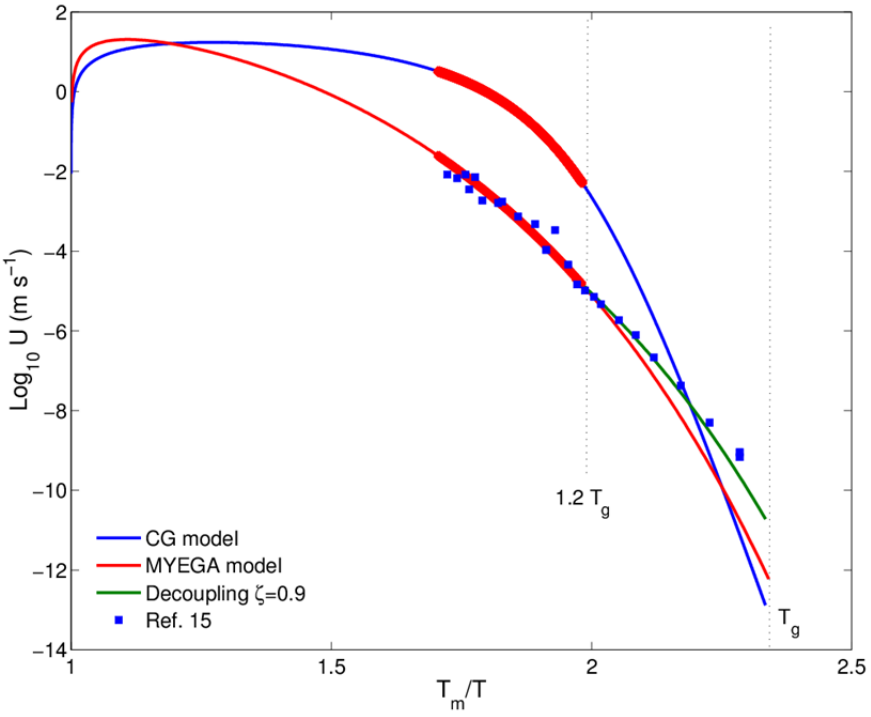

Figure 3.4 Overall temperature dependence of growth rate derived from the MYEGA and CG models. The red curve shows the growth rate of the Ge_7Sb_{93} alloy from T_g to T_m given by Equation 3.2 of the MYEGA model. Blue squares are the growth rate of this alloy, measured by a high speed optical camera and laser acceleration.[15] The green curve shows the growth rate below 1.2 T_g from the MYEGA model, with a decoupling between viscosity and growth rate adopted (ζ=0.9 in $U \propto \eta^{-\zeta}$). The blue curve displays the overall growth rate as function of temperature obtained from the CG model, which results in a 2-3 orders of magnitude overestimation of the growth rate observed in the temperature region of ultrafast DSC. The maximum growth rates given by the MYEGA and CG models are 21 m s^{-1} and 17 m s^{-1}, respectively. The thicker red regions on both curves indicate the temperature region in which the peaks temperatures in the ultrafast DSC have been obtained.

In a perspective of *Wuttig et al.*,[24] it is clearly noticeable in the figure provided that the growth rate derived from the CG model is, for the temperature range of conventional measurements, 3-4 orders of magnitude larger than the independent measured data provided in this figure. Moreover, this model also leads to a substantially larger activation energy for $Ge_2Sb_2Te_5$ within the temperature region where data have been obtained by conventional measurements. For $Ge_2Sb_2Te_5$ thin films it is well-established that the activation energy for crystallization and growth near T_g is in the range 2.2 – 3.0 eV.[7,10,37–42] However, the CG model leads to an unphysically high value beyond 5 eV near T_g (~2.35 T_m/T). These two mismatches thus further strengthen and generalize our conclusion that the CG model seems inappropriate to describe the viscosity and kinetics of PCMs.

3.4 Conclusions

Ultrafast DSC has been employed to study the crystallization kinetics of a growth-dominant phase change material, Ge_7Sb_{93}. Models for growth rate (of phase-change materials) and viscosity (of supercooled liquids) from *Salinga et al*. and *Mauro et al.* were used to analyze the ultrafast DSC data. Fitting these models to the data provides a glass transition temperature of 379 K and a fragility of 65 for this alloy. The overall temperature dependences of the viscosity and growth rate from glass transition to melting temperatures are revealed as well, from which a maximum growth rate of 21 m s^{-1} at ~800 K is extrapolated for supercooled Ge_7Sb_{93} alloy. Next to this model of *Salinga* and *Mauro* (MYEGA) the ultrafast DSC data was also fitted based on the model used by *Orava et al.,* which employs an equation by *Cohen* and *Grest* (CG) to describe the viscosity of glass-forming liquids. In order to test the validity of both models, independent data, in which the growth rate was directly measured as a function of temperature, was used. This test showed that the MYEGA model agrees very well with the data, but the CG model results in orders of magnitude discrepancies. Our analysis shows that the CG model seems inappropriate to describe the viscosity and kinetics of PCMs. This also shows that one has to be careful when deriving crystal growth rates or viscosities on the basis of ultrafast DSC measurements and that some comparison with directly measured growth rates or viscosities is generally required.

Appendix

Thermal lag of the ultrafast DSC

Because of the open structure of the chip sensor where the sample is heated only single sided, it is necessary to estimate the thermal lag of the ultrafast DSC, the most significant source of which includes two parts: 1) delayed heat transfer at the interface between the aluminum stage and sample due to low heat transfer coefficient (h) and 2) temperature gradients inside the sample.

The second factor can be assessed by the dimensionless Biot number:[43]

$$B = \frac{hL}{\kappa} \tag{3.8}$$

where h is the heat transfer coefficient, L the sample thickness and κ the thermal conductivity of the sample materials. The temperature gradient within a sample is negligible if $B << 1$, giving a uniform thermal distribution in the sample. Typical metal casting experiments gives the value of h in the range between 5 and 20 kW m^{-2} K^{-1}.[44] The thickness of the sample we investigate is 200 nm. For amorphous PCMs, κ could be very low (0.17 W m^{-1} K^{-1} for $Ge_{15}Sb_{85}$ at 20 ^{o}C [45]). Taking these values we then obtain a Biot number in the range from 0.005 to 0.05, inferring that the assumption of a uniform temperature distribution within the sample is reasonable. Therefore the dominate concern is the thermal lag due to the thermal transfer at the interface between the chip sensor and the sample.

The thermal lag caused by the heat transfer between the chip sensor and the sample can be estimated by:

$$\Delta T = \frac{C_p L}{h}\Phi \tag{3.9}$$

with C_p the heat capacity per unit volume, L the thickness and Φ the heating rate. We take the value of Sb (no data found for GeSb) thin film: $C_p = 1.39 \times 10^6$ J m^{-3} K^{-1}.[46] With the value for h and L, the ΔT is then in the range 0.5 to 6 K at the maximum heating rate 40 000 K s^{-1}. This thermal lag will not affect the breakdown of the Arrhenius behavior, which starts at 10 000 K s^{-1}, at which the thermal lag is still very small. The main concern of our method is the thermal contact between the sample and the chip sensor, which can vary for different samples as the melt-quench method, which ensures good conformal contact between sample and sensor surface, cannot be applied to our measurements for the phase-change materials.

To confirm a good thermal contact of the non-melt-quenched sample, we also tested the onset temperature (T_{on}) of melting endotherm of scraped-off indium pieces. A thin indium layer with a thickness of 30 nm was deposited on pre-cleaned glass. Then this layer was scraped off and formed small pieces (hardly no flat flakes due to the excellent ductility of indium). Then the small pieces of indium with the sizes of roughly 20×20 μm^2 were then transferred on the chip sensor of ultrafast DSC, following with ultrafast heating at high heating rates. Also here we repeated this measurements for several times at each heating rate and selected the lowest peak temperature values for the best thermal contact as we also do in our measurements of the phase-change materials (PCMs). The temperature at the onset of melting, T_{on}, we measured in this way is 160 °C at a heating rate of 20 000 K s^{-1}, which is similar to the data obtained for melt-quench indium flakes, as depicted in Figure 3.5, indicating that the thermal contact of non-melt-quenched samples do not significantly degrade. Therefore the data we obtained for PCMs (using a non-melt-quenching method) are reliable.

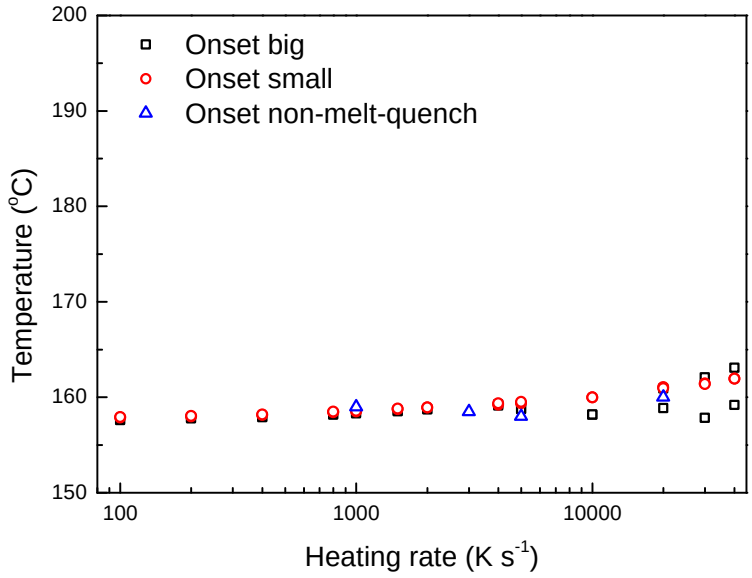

Figure 3.5 Onset temperature of melting endotherm for indium samples prepared by different methods, indicating the good reliability of the method used in this work.

To minimize the possible influence of bad thermal contact between the specimen and the chip sensor, we also repeated measurements many times at each heating rates, especially at high heat rates (above 10 000 K s^{-1}) and then selected the lowest several (3 to 5) peak temperature as the most representative data for fitting.

Optimization process in Kissinger plot

As shown by *Kelton*,[27] the DSC signal is directly proportional to the rate by which the fraction transformed $X(T_i)$ changes. By changing the input parameters in these two growth-rate models also the T_p at a certain heating rate (Φ) can be varied. By adjusting all the parameters, a modeled Kissinger curve can be fitted to experimental data in the Kissinger plot. The fitting procedure used here is the downhill Simplex method due to *Nelder* and *Mead*.[47] In a Kissinger plot the *x* data is equivalent to the $1000/T_p$, where the *y* data correspond to $\ln(\Phi/T_p^2)$. The χ^2 in the fitting procedure was defined as the difference between the experimentally measured data $x(x_i)$ and the modeled data $x(x_{\mathrm{mod}})$ in the Kissinger plot: $\chi^2 = \sum_{i=1}^{k}(x_i - x_{\mathrm{mod}})^2$, because in the Kissinger plot the *y* data hardly changes at a certain Φ for different T_p . In the Simplex method starting estimations for the fitting parameters have to be provided. It turned out essential to have a reasonable starting value for the number density of nuclei.

Estimation of number density of nuclei *N*

During fitting the data in the Kissinger plot by means of the growth models and JMAK theory, we find that the nucleation density *N* impacts the final fitting results. For instance, the fitting fragility *m* is shifted from 65 to 95 in the MYEGA model if the *N* is exaggeratedly lowered from 10^{16} m^{-3} to 10^{10} m^{-3}. Interestingly, this change in *N* does not affect the value of the glass transition temperature T_g obtained by fitting the data in the Kissinger plot. Figure 3.6 shows in an Angell plot the result of this fitting with these two fixed values of *N*.

Because of the importance to have a reasonable estimate for *N*, it is required to have a reasonable approximation of the nuclei numbers during heating in the ultrafast DSC. The strength of our current approach is that we have this estimate based on our earlier work employing a high speed optical camera to monitor the nucleation and growth of crystals in the 200 nm thick Ge_7Sb_{93} films.[15] The phase transition of these films was investigated via isochronal heating on a ceramic heater at a Φ of 10 °C min^{-1}. Observable nuclei develop at about 130 °C. Figure 3.7 a-b show the change of nuclei with temperature, increasing for the area observed from 123 at 133.3 °C to 147 at 142.3 °C. The number of nuclei thus only increases by ~20%. An approximated value for *N* is achieved as $\sim 4.1 \times 10^{14}$ m^{-3} at 142 °C when a 3-dimensional growth model is adopted for the crystals and considering the thickness of this film (200 nm). From the video made from this measurement, it is clear that the number of nuclei hardly increase after 140 °C for this Φ . After the initial nucleation

below 135 °C, the dominant process of crystallization is thus growth of crystals. Moreover, in all our measurements of crystallization of Ge_7Sb_{93} films we observed that all crystals observed in a certain area tend to have the same size. These observations thus show that the constant nuclei assumption in the numerical calculations via JMAK theory is justified.

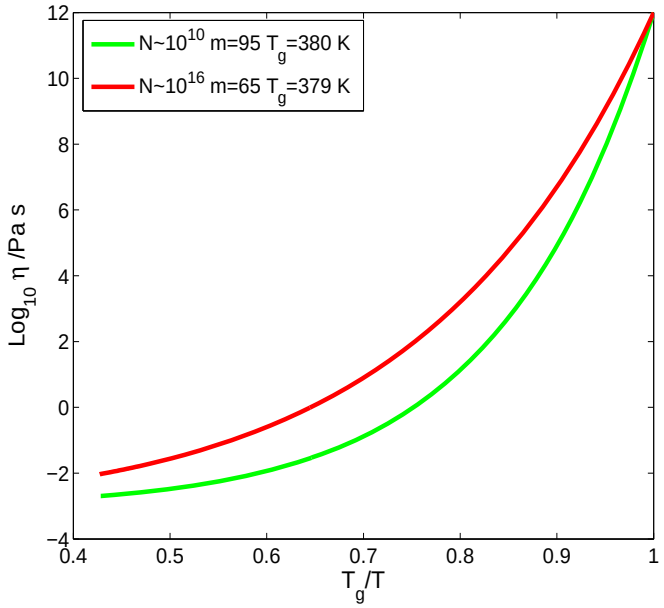

Figure 3.6 Angell plot with different number density of nuclei N. This figure displays the viscosity as function of temperature for two *N* values, i.e. 10^{10} m^{-3} to 10^{16} m^{-3} in order to demonstrate the importance to have a reasonable estimate for *N*. While the fitted T_g scarcely changed (~380 K), the m changes remarkably from 95 to 65.

However, in another measurement, it is found that scraping off the Ge_7Sb_{93} films remarkably enlarges the possibility of nucleation as shown in Figure 3.7c, where areas which have been scratched (and which probably experienced compressive stress) experience earlier nucleation than the surrounding PCM under isothermal heating, resulting in a greater value for *N*. Accelerated crystallization by applying modest compressive stresses to Ge_6Sb_{94} or Ge_7Sb_{93} films has also been demonstrated by our previous work.[48] Stress-induced crystallization of $Ge_{15}Sb_{85}$ has also been discussed by *Shakhvorostov et al.*.[49] Therefore, the real *N* in the ultrafast DSC measurements must be larger than 10^{14} m^{-3}. On the other hand, with an *N* value larger than 10^{17} m^{-3} the data in the Kissinger plot could not be fitted. So, the reasonable region of *N* values is 10^{15} to 10^{16} m^{-3} in our fitting, and the one we used is 10^{16} m^{-3}. Note this is the starting value employed in the fitting procedure using the downhill Simplex method and therefore still some minor adjustment of number density of nuclei *N* is possible as a result of the fitting procedure. For this fitting a value of 5×10^{16} m^{-3} is derived for *N*.

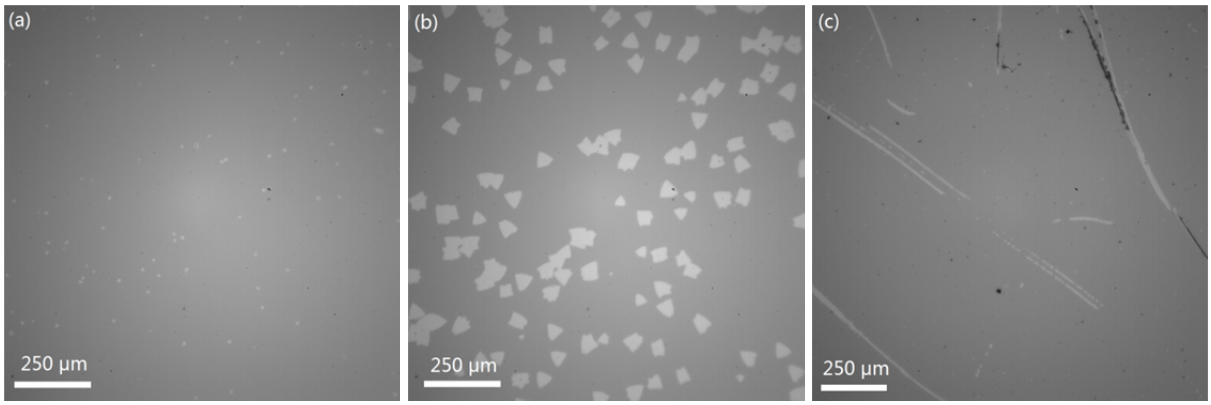

Figure 3.7 Ge_7Sb_{93} films under isochronal heating. (a) shows the nuclei number of 123 at 133.3 °C; (b) shows the number of nuclei changes to 147 at 142.3 °C. From (a) and (b) the density of nuclei can be derived for both 2-dimensional (8.2×10^{7} m^{-2}) and 3-dimensional (4.1×10^{14} m^{-3}) crystal growth for JMAK theory at 142 °C, as the thickness of the film is 200 nm. (c) shows the pressure-induced nucleation on Ge_7Sb_{93} films. (c) The scratches made by a hair nucleate earlier than the surrounding materials under isothermal heating at 125°C , with an obviously higher nuclei density.

Effect of the *A* parameter in the *Cohen* & *Grest* expression for determining the growth rate

In Figure 3.8, the influence of the value of *A* in the CG model (see Equation 3.5) on the growth rate is shown. The blue curve shows the growth rate derived from the Stokes-Einstein equation, identical to the one in Figure 3.4, leading to a maximum growth rate (U_m) of 17 m s^{-1}. The green curve in this figure is derived when *A* is set to the 0, which is the value employed in the fitting of the Kissinger plot (Figure 3.2). A U_m of 0.17 m s^{-1} is obtained here. Then, the value of *A* is adapted in order to match the independent data from Ref. 15. Then *A* becomes -0.4 and the corresponding growth rate curve is the khaki one in Figure 3.8. It is nicely shown that this modeled growth rate matches well with the independent data in the limited measurement region of the ultrafast DSC which is between 450 and 505 K, but still leads to a poor fit for temperatures below 450 K. Moreover, this *A* value results in a unacceptable low value of U_m (0.07 m s^{-1}). From the original equation and from the graph it is obvious that the effect of *A* in the C&G model is that it only changes the absolute value of the of the growth rate and thus only results in a vertical shift of the curves in Figure 3.8. The present results thus strongly suggest that this C&G model is not suitable to describe the growth rate of PCMs, at least for the growth dominated GeSb alloy. However, quite similar discrepancies between modelled and experimental results are observable for the nucleation dominated $Ge_2Sb_2Te_5$ alloy in Figure 1 of Ref. 24. Therefore, indeed, it appears justified to question the appropriateness of the CG model for PCMs in general.

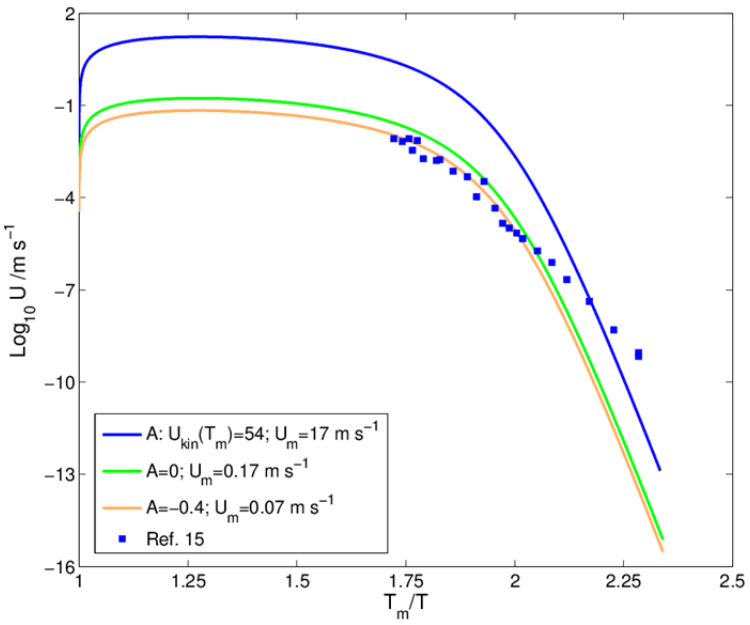

Figure 3.8 Growth rate from the CG model for different values of parameter *A*. The green curve is identical to the one shown in the Figure 3.4 in the main text, which leads to a maximum growth rate value (U_m) of 17 m s^{-1}. The khaki curve relates to the value *A*=0, which is the one used for fitting in the Kissinger plot. A U_m of 0.17 m s^{-1} is obtained. Then the value of *A* is set to make the modeled growth rate match to the independent data. *A*=-0.4, the green curve is obtained as the growth rate. Although good match to the data can be seen, an unacceptable value of U_m (0.07 m s^{-1}) is derived here.

References

(1) Raoux, S.; Welnic, W.; Ielmini, D. *Chem. Rev.* **2010**, *110* (1), 240–267.
(2) Wuttig, M.; Yamada, N. *Nat. Mater.* **2007**, *6* (11), 824–832.
(3) Park, J.; Kim, M. R.; Choi, W. S.; Seo, H.; Yeon, C. *Jpn. J. Appl. Phys.* **1999**, *38* (8R), 4775.
(4) Coombs, J. H.; Jongenelis, A. P. J. M.; Es-Spiekman, W. van; Jacobs, B. a. J. *J. Appl. Phys.* **1995**, *78* (8), 4906–4917.
(5) Kooi, B. J.; Hosson, J. T. M. D. *J. Appl. Phys.* **2004**, *95* (9), 4714–4721.
(6) Rocca, J.; Erazú, M.; Fontana, M.; Arcondo, B. *J. Non-Cryst. Solids* **2009**, *355* (37–42), 2068–2073.
(7) Kalb, J.; Spaepen, F.; Wuttig, M. *Appl. Phys. Lett.* **2004**, *84* (25), 5240–5242.
(8) Kooi, B. J.; Groot, W. M. G.; Hosson, J. T. M. D. *J. Appl. Phys.* **2004**, *95* (3), 924–932.
(9) Raoux, S.; Jr, C. C.; Krusin-Elbaum, L.; Jordan-Sweet, J. L.; Virwani, K.; Hitzbleck, M.; Salinga, M.; Madan, A.; Pinto, T. L. *J. Appl. Phys.* **2009**, *105* (6), 064918.
(10) Friedrich, I.; Weidenhof, V.; Njoroge, W.; Franz, P.; Wuttig, M. *J. Appl. Phys.* **2000**, *87* (9), 4130–4134.
(11) Hegedüs, J.; Elliott, S. R. *Nat. Mater.* **2008**, *7* (5), 399–405.
(12) Matsunaga, T.; Akola, J.; Kohara, S.; Honma, T.; Kobayashi, K.; Ikenaga, E.; Jones, R. O.; Yamada, N.; Takata, M.; Kojima, R. *Nat. Mater.* **2011**, *10* (2), 129–134.
(13) Zhang, W.; Ronneberger, I.; Zalden, P.; Xu, M.; Salinga, M.; Wuttig, M.; Mazzarello, R. *Sci. Rep.* **2014**, *4*.
(14) Sosso, G. C.; Colombo, J.; Behler, J.; Del Gado, E.; Bernasconi, M. *J. Phys. Chem. B* **2014**, *118* (47), 13621–13628.
(15) Eising, G.; Van Damme, T.; Kooi, B. J. *Cryst. Growth Des.* **2014**, *14* (7), 3392–3397.
(16) Salinga, M.; Carria, E.; Kaldenbach, A.; Bornhöfft, M.; Benke, J.; Mayer, J.; Wuttig, M. *Nat. Commun.* **2013**, *4*.
(17) Orava, J.; Greer, A. L.; Gholipour, B.; Hewak, D. W.; Smith, C. E. *Nat. Mater.* **2012**, *11* (4), 279–283.
(18) Cohen, M. H.; Grest, G. S. *Phys. Rev. B* **1979**, *20* (3), 1077–1098.
(19) A.N. Kolmogorov. *Bull Acad Sci USSR Math Ser* **1937**, *1*, 355–359.
(20) W.A. Johnson, R.F. Mehl. *Trans Aime* **1939**, *135* (8), 396–415.
(21) Avrami, M. *J. Chem. Phys.* **1939**, *7* (12), 1103–1112.
(22) Avrami, M. *J. Chem. Phys.* **1940**, *8* (2), 212–224.
(23) Avrami, M. *J. Chem. Phys.* **1941**, *9* (2), 177–184.
(24) Wuttig, M.; Salinga, M. *Nat. Mater.* **2012**, *11* (4), 270–271.
(25) Orava, J.; Hewak, D. W.; Greer, A. L. *Adv. Funct. Mater.* **2015**, n/a-n/a.
(26) Eising, G.; Niebuur, B.-J.; Pauza, A.; Kooi, B. J. *Adv. Funct. Mater.* **2014**, *24* (12), 1687–1694.
(27) Kelton, K. F. *Mater. Sci. Eng. A* **1997**, *226–228*, 142–150.
(28) Vermeulen, P. A.; Momand, J.; Kooi, B. J. *J. Chem. Phys.* **2014**, *141* (2), 024502.
(29) Kissinger, H. E. *Anal. Chem.* **1957**, *29* (11), 1702–1706.
(30) Thompson, C. V.; Spaepen, F. *Acta Metall.* **1979**, *27* (12), 1855–1859.
(31) Kalb, J. A.; Wuttig, M. Publikationsserver der RWTH Aachen University 2006.
(32) Olesinski, R. W.; Abbaschian, G. J. *Bull. Alloy Phase Diagr.* **1986**, *7* (3), 219–222.
(33) Mauro, J. C.; Yue, Y.; Ellison, A. J.; Gupta, P. K.; Allan, D. C. *Proc. Natl. Acad. Sci.* **2009**, *106* (47), 19780–19784.
(34) Kalb, J. a.; Wuttig, M.; Spaepen, F. *J. Mater. Res.* **2007**, *22* (03), 748–754.
(35) Derk Jan Adelerhof, European Phase Change and Ovonics Symposium, 2004, epcos.org (http://www.epcos.org/library/Library2004.htm).
(36) Ediger, M. D. *Annu. Rev. Phys. Chem.* **2000**, *51* (1), 99–128.

(37) Ohshima, N. *J. Appl. Phys.* **1998**, *83* (10), 5244–5250.
(38) Privitera, S.; Bongiorno, C.; Rimini, E.; Zonca, R. *Appl. Phys. Lett.* **2004**, *84* (22), 4448–4450.
(39) Morales-Sánchez, E.; Prokhorov, E. F.; González-Hernández, J.; Mendoza-Galván, A. *Thin Solid Films* **2005**, *471* (1–2), 243–247.
(40) Redaelli, A.; Pirovano, A.; Tortorelli, I.; Ielmini, D.; Lacaita, A. L. *IEEE Electron Device Lett.* **2008**, *29* (1), 41–43.
(41) Choi, Y.; Jung, M.; Lee, Y.-K. *Electrochem. Solid-State Lett.* **2009**, *12* (7), F17–F19.
(42) Tominaga, J.; Shima, T.; Fons, P.; Simpson, R.; Kuwahara, M.; Kolobov, A. *Jpn. J. Appl. Phys.* **2009**, *48* (3S1), 03A053.
(43) Incropera, F. P.; De Witt, D. P. **1985**.
(44) Şahin, H. M.; Kocatepe, K.; Kayıkcı, R.; Akar, N. *Energy Convers. Manag.* **2006**, *47* (1), 19–34.
(45) Risk, W. P.; Rettner, C. T.; Raoux, S. *Appl. Phys. Lett.* **2009**, *94* (10), 101906.
(46) Kalb, J. A. **2006**.
(47) Nelder, J. A.; Mead, R. *Comput. J.* **1965**, *7* (4), 308–313.
(48) Eising, G.; Pauza, A.; Kooi, B. J. *Cryst. Growth Des.* **2013**, *13* (1), 220–225.
(49) Shakhvorostov, D.; Nistor, R. A.; Krusin-Elbaum, L.; Martyna, G. J.; Newns, D. M.; Elmegreen, B. G.; Liu, X.; Hughes, Z. E.; Paul, S.; Cabral, C.; Raoux, S.; Shrekenhamer, D. B.; Basov, D. N.; Song, Y.; Müser, M. H. *Proc. Natl. Acad. Sci.* **2009**, *106* (27), 10907–10911.